

Majorana fermion arcs and the local density of states of UTe_2

Yue Yu,¹ Vidya Madhavan,² and S. Raghu^{1,3}

¹*Department of physics, Stanford University, Stanford, California 94305, USA*

²*Department of Physics and Materials Research Laboratory,
University of Illinois Urbana-Champaign, Urbana, IL, USA*

³*SLAC National Accelerator Laboratory, 2575 Sand Hill Road, Menlo Park, CA 94025, USA*

UTe_2 is a leading candidate for chiral p-wave superconductivity, and for hosting exotic Majorana fermion quasiparticles. Motivated by recent STM experiments in this system, we study particle-hole symmetry breaking in chiral p-wave superconductors. We compute the local density of states from Majorana fermion surface states in the presence of Rashba surface spin-orbit coupling, which is expected to be sizeable in heavy-fermion materials like UTe_2 . We show that time-reversal and surface reflection symmetry breaking lead to a natural pairing tendency towards a triplet pair density wave state, which naturally can account for broken particle-hole symmetry.

Introduction - Odd parity superconductors are notable for having a rich pattern of broken symmetries^{1,2} and non-trivial topological properties³⁻⁶, making them promising avenues for the realization of Majorana fermion modes. Odd parity superconductivity is inevitably unconventional, arising from electron-electron repulsion rather than from a more conventional electron-phonon pairing mechanism⁷. Thus, they tend to be realized in strongly correlated systems with complex phase diagrams and competing ordering tendencies. While odd parity superconductivity has been observed in relatively few systems, UTe_2 is a strong candidate: it exhibits several striking phenomena including an extraordinarily large upper critical field⁸, reentrant superconductivity⁹ and broken time-reversal symmetry¹⁰.

Recent scanning tunneling spectroscopy measurements¹¹ of UTe_2 have revealed an unusual signature that is yet to be explained. STM spectra obtained near step edges in the superconducting phase show broken particle-hole symmetry (PHS). This observation is sharply distinct from classical BCS superconductors, which exhibit an emergent PHS at energies below the gap: the difference between adding and removing an electron is a Cooper pair, which is unobservable in a conventional Cooper pair condensate. Since STM directly measures local density of states, these unusual edge modes may be signatures of putative chiral Majorana modes, and thus, it is of central interest to understand these experimental observations.

A clue to understanding the question of broken PHS in a superconductor comes from studies of materials with non-zero Cooper pair momentum¹²⁻¹⁴ which are typically associated with a pair density wave (PDW) modulation. It is well-known that when superconductivity is accompanied by charge modulation, PHS breaking usually occurs. It is thus possible that the observations of broken PHS in UTe_2 can be explained by the development of inhomogeneous superconductivity near the surface. In this letter, we show how PHS breaking can emerge from finite momentum Cooper pairing near the surface of an odd parity chiral superconductor.

Symmetry considerations - Since the PDW state is not

a generic weak-coupling instability of a Fermi liquid, one cannot predict unambiguously when it might occur. Nevertheless, there are some reliable rules-of-thumb. When the normal state has both time-reversal and inversion symmetry, the spectrum consists of Kramers degenerate pairs at momenta ($\pm\mathbf{k}$) and uniform superconductivity is overwhelmingly preferred in the weak-coupling limit. In this case, the BCS superconductor is labeled by a “pseudospin” degree of freedom stemming from the normal state Kramers’ degeneracy. Thus, to tilt the balance in favor of the PDW state, either inversion or time-reversal symmetry ought to be broken in the normal state. For instance, a Zeeman field can help stabilize a PDW state in pseudospin singlet superconductors, as is believed to be the case in CeCoIn_5 ^{15,16}. Similarly, a PDW state in an odd parity superconductor can be stabilized by breaking inversion (or reflection) symmetry, as we explain below.

In the case of UTe_2 , both time-reversal and inversion symmetries occur in the normal state in the *bulk*. However, spatial reflection symmetry is broken at the *surface*. This leads to a Rashba spin-orbit coupling (SOC) which decays in strength away from the surface. If this decay length is sufficiently long compared to the superconducting correlation length, or if the SOC itself is sufficiently strong (as is likely the case in UTe_2 due to the large bulk atomic SOC scales), Majorana surface modes will be strongly affected by the reflection symmetry breaking at the surface, which results in a PDW component to the condensate. The symmetry considerations therefore suggest that the STM observations of broken PH in UTe_2 may be attributed to non-uniform superconductivity induced at the surface by sizeable Rashba SOC.

Model- We first provide an explicit example that illustrates how non-uniform superconductivity is induced by local inversion symmetry breaking. Since the electronic structure of UTe_2 remains poorly understood we instead consider a single band effective description. Let us suppose that the overwhelming pairing tendency is in the odd parity pseudospin triplet channel without a PDW component. Deep in the bulk, the superconductor is de-

scribed by mean-field Hamiltonian of the following form:

$$\begin{aligned}
H &= H_0 + H_\Delta + H_{Rashba} \\
H_0 &= \sum_{\mathbf{k},\sigma} (E_{\mathbf{k}\sigma} - \mu) c_{\mathbf{k}\sigma}^\dagger c_{\mathbf{k}\sigma} \\
H_\Delta &= \sum_{\mathbf{k},\sigma,\sigma'} \Delta_{\sigma\sigma'\mathbf{k}} c_{\mathbf{k},\sigma} c_{-\mathbf{k},\sigma'} + \text{h.c.} \quad (1)
\end{aligned}$$

We assume that the system has lattice translation symmetry. Thus, $c_{\mathbf{k}\sigma}$ destroys an electron with crystal momentum \mathbf{k} , and pseudospin σ . The band energies $E_{\mathbf{k}\sigma}$ are time-reversal symmetric and appropriate for an orthorhombic crystal, such as that of UTe_2 . Pseudospin-triplet superconducting states are then characterized by a matrix-valued order parameter $\Delta_{\sigma\sigma'\mathbf{k}}$.

Near the surface, superconductivity is subject to a sizeable Rashba spin-orbit coupling due to the breaking of reflection symmetry. Letting \hat{n} be the vector normal to a surface, the Rashba SOC Hamiltonian usually takes the form

$$H = \lambda \sum_{\mathbf{k}\sigma} \hat{n} \cdot (\mathbf{k} \times \boldsymbol{\sigma}). \quad (2)$$

In an orthorhombic crystal, such as UTe_2 , the lack of a fourfold rotational axis results in a less restrictive form of Rashba SOC. Letting $\hat{n} = \hat{y}$, the surface Rashba SOC of an orthorhombic system has the form

$$H_{Rashba} = -\lambda k_x S_z + \lambda' k_z S_x, \quad (3)$$

with generically distinct values of λ and λ' . In what follows, we will neglect spatial decay of λ, λ' into the bulk and treat them as constant parameters of the surface Hamiltonian. In addressing the effect of these surface Fermi surface distortions on superconductivity, we assume that the superconducting gap scale is small compared to the Rashba coupling, as is usually the case for BCS superconductors.

The existence of an induced PDW is most clearly demonstrated in the extreme orthorhombic limit where $\lambda' \ll \lambda$. In this limit, the pseudospin S_z is well approximated as a good quantum number. Moreover, $\Delta_{\uparrow\uparrow}$ and $\Delta_{\downarrow\downarrow}$ condensate now “live” on separate Fermi surfaces as shown in Fig. 1, and therefore prefer non-zero centers of mass momenta $\mathbf{q}_\pm \equiv (\mathbf{q}_{x\pm}, \mathbf{0}, \mathbf{0})$. And it remains energetically more favorable for the condensate in the $\Delta_{\uparrow\downarrow}$ channel to have zero center of mass momentum. Since chiral p-wave state breaks TRS, in general $\mathbf{q}_+ \neq -\mathbf{q}_-$. If all three channels are ordered, there will be three distinct condensate momenta, while two condensate momenta are already sufficient for the PDW^{13,14}. The difference between those two momenta determines the orientation and periodicity of PDW:

$$\Delta(\mathbf{x}) \sim \cos\left(\frac{1}{2}\Delta\mathbf{q} \cdot \mathbf{x}\right) \quad (4)$$

Since the three pairing channels have different condensate momenta, they will naturally compete with each

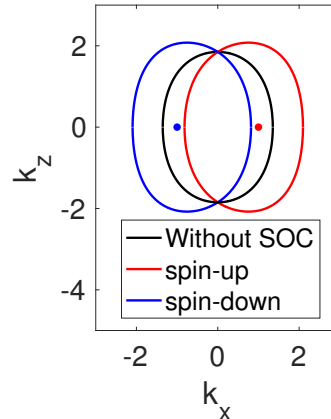


FIG. 1: Projected Fermi surfaces onto (k_x, k_z) plane for (Black line) Fermi surface in the absence of Rashba SOC, as well as (Red, Blue) pseudospin-up, down Fermi surface under Rashba SOC. Band dispersion is $E_{\mathbf{k}\sigma} = \sum_i \frac{k_i^2}{2m_i} + \sum_i \frac{k_i^4}{2n_i}$ for the plots, with $m_x = 1, m_y = 2, m_z = 3, n_x = 20, n_y = 40, n_z = 60, \mu = 1, \lambda = 0.8$ and $\lambda' = 0$. Blue and red dots are the approximate position for \mathbf{q}_\pm .

other. In this $\lambda' \ll \lambda$ limit, if $\Delta_{\uparrow\downarrow}$ channel is suppressed by competition, the remaining competition between $\Delta_{\uparrow\uparrow}$ and $\Delta_{\downarrow\downarrow}$ channel will be weak; therefore it is energetically easier for these two condensates to coexist. Other coexisting scenarios are more difficult to happen, but still possible under certain pairing interactions.

The complementary extreme limit $\lambda' \gg \lambda$, can be handled in the same way upon exchanging the x and z coordinates. In terms of the original coordinate system, the resulting PDW state would now have its center of mass momenta along the z -direction.

As we deviate from the limit $\lambda' \ll \lambda$, the first corrections from λ' would be to alter the shape of Fermi surfaces and the momenta of the PDW phase, but we expect the PDW phases to survive to a finite range of λ'/λ . Similarly, we expect the PDW in the complementary limit to survive up to a finite range of λ/λ' . Since the two PDW phases in either extreme have distinct center of mass momenta, there are a variety of possibilities for intermediate λ'/λ . There could be a direct first-order transition where the PDW momenta jump abruptly from one phase to the other, or a coexistence phase with both sets of PDW momenta present. There could also be an intermediate phase without PDW order. The correct scenario needs to be determined by the detail of the Fermi surface and the pairing interactions, while the λ/λ' ratio is determined by the orientation of the measured surface. But we can state with certainty that the PDW phases obtained in the limit of extreme orthorhombicity do not require fine-tuning.

Chiral edge modes and LDOS - Next we consider the quasiparticle spectrum in the strongly orthorhombic limit with $\lambda \neq 0$ and $\lambda' = 0$, assuming all three channels are ordered. Since translational symmetry is broken in the

PDW, the Bogoliubov–de Gennes (BdG) Hamiltonian is not block-diagonal, and truncation is needed for concrete computations. To illustrate the essential idea at a qualitative level, we truncate the Hamiltonian to the following 4×4 form to include just two PDW momenta q_+ , q_- :

$$H = \sum_{\mathbf{k}} \Phi_{\mathbf{k}}^\dagger h_{\mathbf{k}} \Phi_{\mathbf{k}}$$

$$\Phi_{\mathbf{k}}^\dagger = [c_{\mathbf{k}\uparrow}^\dagger \quad c_{\mathbf{k}+\mathbf{q}_-\downarrow}^\dagger \quad c_{-\mathbf{k}+\mathbf{q}_+\uparrow} \quad c_{-\mathbf{k}\downarrow}]$$

$$h_{\mathbf{k}} = \begin{bmatrix} \varepsilon_{\mathbf{k}\uparrow} & 0 & \Delta_{\uparrow\uparrow}(\mathbf{k}) & \Delta_{\uparrow\downarrow}(\mathbf{k}) \\ 0 & \varepsilon_{\mathbf{k}+\mathbf{q}_-\downarrow} & 0 & \Delta_{\downarrow\downarrow}(\mathbf{k}+\mathbf{q}_-) \\ \Delta_{\uparrow\uparrow}^*(\mathbf{k}) & 0 & -\varepsilon_{-\mathbf{k}+\mathbf{q}_+\uparrow} & 0 \\ \Delta_{\uparrow\downarrow}^*(\mathbf{k}) & \Delta_{\downarrow\downarrow}^*(\mathbf{k}+\mathbf{q}_-) & 0 & -\varepsilon_{-\mathbf{k}\downarrow} \end{bmatrix} \quad (5)$$

with the following simple normal state dispersion:

$$\varepsilon_{\mathbf{k}\uparrow} = \frac{k^2}{2m} - \mu - \lambda k_x; \quad \varepsilon_{\mathbf{k}\downarrow} = \frac{k^2}{2m} - \mu + \lambda k_x \quad (6)$$

The anti-commutation relationship imposes the following constraint on the pairing function:

$$\begin{aligned} \Delta_{\uparrow\uparrow}(\mathbf{k}) &= -\Delta_{\uparrow\uparrow}(\mathbf{q}_+ - \mathbf{k}) \\ \Delta_{\uparrow\downarrow}(\mathbf{k}) &= -\Delta_{\uparrow\downarrow}(-\mathbf{k}) \\ \Delta_{\downarrow\downarrow}(\mathbf{k}) &= -\Delta_{\downarrow\downarrow}(\mathbf{q}_- - \mathbf{k}) \end{aligned} \quad (7)$$

It should be noted that much larger matrices and a realistic band structure are required for future quantitative analysis. The result for 8×8 truncation can be found in the appendix.

Using the above Hamiltonian, we compute the surface bound state spectrum and the local density of states to validate the qualitative picture above of broken PHS. We will compare the results in (1) the uniform $\mathbf{q} = \mathbf{0}$ state without Rashba SOC, and (2) the non-uniform PDW state with Rashba SOC. For simplicity, we take the same “ $p_x + ip_y$ ” pairing state for both cases:

$$\begin{aligned} \Delta_{\uparrow\uparrow}(\mathbf{k}) &= \Delta_1 k_z \\ \Delta_{\uparrow\downarrow}(\mathbf{k}) &= \Delta_{\downarrow\uparrow}(\mathbf{k}) = \Delta_2 k_x + i\Delta_3 k_y \\ \Delta_{\downarrow\downarrow}(\mathbf{k}) &= \Delta_4 k_z, \end{aligned} \quad (8)$$

with real coefficient Δ_i .

Given a BdG Hamiltonian, the existence of chiral surface-bound states is governed by the regions in the bulk Fermi surface where the pairing gap closes. In a three-dimensional chiral p-wave state, a Fermi surface that is closed and encloses time-reversal invariant momenta will necessarily have point nodes corresponding to bulk Majorana fermion excitations. With the parameters chosen in the caption of Fig.2, these point nodes are located on the (k_x, k_z) plane, shown as the black dots in the upper panel of Fig.2. They appear in pairs, with opposite momenta, due to both PH symmetry and inversion symmetry.

For surface-bound states on the xz plane, k_x and k_z are still good quantum numbers and label the eigenenergies,

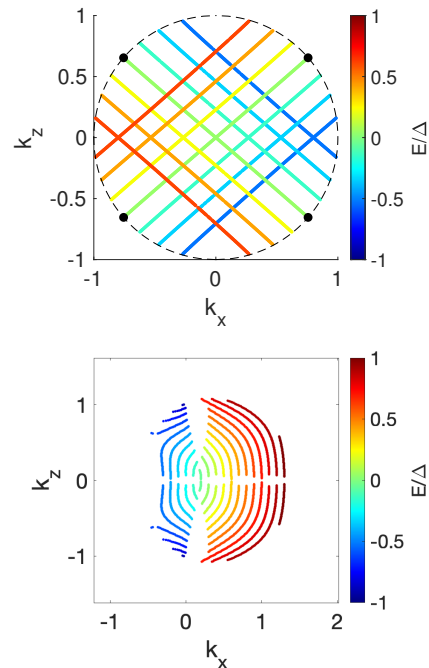


FIG. 2: (Top) Arc states without SOC ($\lambda = 0$, $q_{x\pm} = 0$). (bottom) Arc states in the non-uniform state ($\lambda = 0.8$, $q_{x+} = 0.8$, $q_{x-} = -0.6$). Black dots denote the point nodes, located on (k_x, k_z) plane for the chosen parameters. $m = 0.5$, $\mu = 1$, $\Delta_1 = 0.2$, $\Delta_2 = \Delta_3 = \Delta_4 = 0.15$ are used for both cases. Dashed lines are the boundary of the projected normal state Fermi surface. $\Delta = 0.2$ is used for the colorbar.

while the state decays along the y-direction into the bulk. For a fixed energy E , the states satisfying $E(k_x, k_z) = E$ form arcs in (k_x, k_z) plane. If the system has Majorana point nodes, there are zero-energy Majorana arc states, connecting two projected point nodes¹⁷.

For the uniform $\mathbf{q} = \mathbf{0}$ state (upper panel of Fig.2), zero-energy Majorana arc states (with $E(k_x, k_z) = 0$) are denoted in green lines, which are surrounded by non-zero energy arc states in other colors. Particle-hole symmetry is preserved. For example, any state on the red arc has a counterpart on the blue arc, with opposite energy and opposite momentum. For the non-uniform PDW state (lower panel), PH symmetry is broken, and there is no correspondence between positive energy states and negative energy states.

Since k_x and k_z are now good quantum numbers, number of states in unit square in (k_x, k_z) plane is uniform. This allows us to find the quasi-particle local density of states (LDOS), contributed by arc states:

$$\rho_{LDOS}(E) = \sum_{k_x k_z} \delta(E - E(k_x, k_z)) \quad (9)$$

The results can be found in Fig.3. LDOS in the uniform state is symmetric and peaked at $E = 0$, while LDOS in the PDW state is asymmetric. The shape of LDOS depends on the details of the Fermi surface, the pairing function, and the orientation of the measured surface.

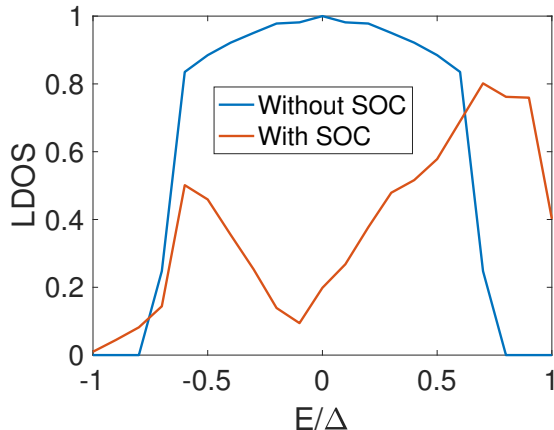


FIG. 3: Density of states contributed by arc states. In the absence of Rashba SOC (blue line), system has particle-hole symmetry; and LDOS is symmetric. For non-uniform states under Rashba SOC (Red line), particle hole symmetry is broken with a peak in DOS at non-zero energy. Same parameters are used as in Fig. 2. $\Delta \equiv 0.2$ is used.

It should be noted that signal in STM is contributed by both surface-bound states and also bulk states, so the above analysis is far from complete. Even among the surface states, states closer to the bulk nodes will have a longer decay lengths, i.e. less localized near the surface. This may affect sensitivity to STM. Therefore, a more detailed calculation is required for the quantitative description of the STM experiment.

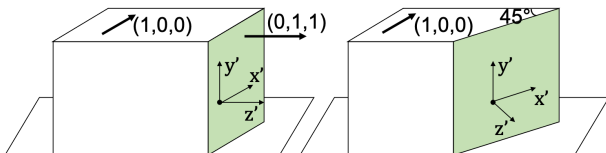


FIG. 4: Experimental settings on UTe_2 . Measurements are performed on the green surfaces. For system on the left, particle-hole symmetry is broken as it approaches the top surface. For system on the right, particle-hole symmetry is found to be unbroken. Number vectors follow the crystal axes.

Discussions on the recent STM experiment - In the STM experiment of Ref. 11, the LDOS near the step edge on $(0, 1, 1)$ and $(0, -1, -1)$ surfaces (shown in green in Fig.4) broke PHS. In the present context, the observations can be understood by postulating that the strength of the Rashba SOC is stronger near the step edge. This is a reasonable hypothesis, since the confining potential is stronger, and the chiral surface modes are therefore more localized near the step edge. Thus, we expect the PDW fraction to be higher in such regions.

For LDOS on $(0, 1, 1)$ surface, there is a dip and peak at around opposite energies. When comparing results on $(0, 1, 1)$ with $(0, -1, -1)$ surface, the position of dips and peaks is reversed. Analysis on these two surfaces can be found in the appendix, but we did not find any symmetry explanations for these findings, since the only symmetry relating positive and negative energies is PH symmetry, which is broken. On the right figure of Fig.4, PH symmetry is found to be preserved on this “45°” step edge. One possible explanation is the absence of PDW since here the Rashba SOC is different from the previous surfaces. A more quantitative analysis based on realistic Fermi surface and pairing functions may explain these observations.

Summary - We study the effect of Rashba spin-orbit coupling on the local density of states of chiral p-wave superconductors. We point to a natural pairing tendency towards the triplet-PDW state, in the absence of an external magnetic field and without bulk inversion symmetry breaking. We find that the LDOS near step edges shows broken PHS. Our methods are readily applicable to various experiments, including the recent STM experiment on UTe_2 , and lend increasing support to the notion that this system hosts chiral p-wave superconductivity with Majorana fermion quasiparticle states.

Acknowledgments - We thank D. Agterberg, B. Bradlyn, S.-B. Chung, S. Kivelson and F. Zhou for helpful discussions. SR is supported by the Department of Energy, Office of Basic Energy Sciences, Division of Materials Sciences and Engineering, under contract No. DE-AC02-76SF00515.

¹ A. J. Leggett, Rev. Mod. Phys. **47**, 331 (1975), URL <https://link.aps.org/doi/10.1103/RevModPhys.47.331>.

² D. Vollhardt and P. Wolfe, *The superfluid phases of helium 3* (Courier Corporation, 2013).

³ X.-L. Qi and S.-C. Zhang, Reviews of Modern Physics **83**, 1057 (2011).

⁴ M. Leijnse and K. Flensberg, Semiconductor Science and Technology **27**, 124003 (2012).

⁵ M. Sato and Y. Ando, Reports on Progress in Physics **80**, 076501 (2017), URL <https://doi.org/10.1088/1361-6633/aa6ac7>.

⁶ A. K. C. Cheung and S. Raghu, Phys. Rev. B **93**, 134516 (2016), URL <https://link.aps.org/doi/10.1103/PhysRevB.93.134516>.

⁷ M. Sigrist and K. Ueda, Rev. Mod. Phys. **63**, 239 (1991), URL <https://link.aps.org/doi/10.1103/RevModPhys.63.239>.

⁸ D. Aoki, A. Nakamura, F. Honda, D. Li, Y. Homma, Y. Shimizu, Y. J. Sato, G. Knebel, J.-P. Brison, A. Pourret, et al., Journal of the Physical Society of Japan **88**, 043702 (2019).

⁹ S. Ran, I.-L. Liu, Y. S. Eo, D. J. Campbell, P. M. Neves, W. T. Fuhrman, S. R. Saha, C. Eckberg, H. Kim, D. Graf,

- et al., *Nature Physics* **15**, 1250 (2019).
- ¹⁰ I. M. Hayes, D. S. Wei, T. Metz, J. Zhang, Y. S. Eo, S. Ran, S. R. Saha, J. Collini, N. P. Butch, D. F. Agterberg, et al., arXiv preprint arXiv:2002.02539 (2020).
- ¹¹ L. Jiao, S. Howard, S. Ran, Z. Wang, J. O. Rodriguez, M. Sigrist, Z. Wang, N. P. Butch, and V. Madhavan, *Nature* **579**, 523 (2020).
- ¹² P. Fulde and R. A. Ferrell, *Phys. Rev.* **135**, A550 (1964), URL <https://link.aps.org/doi/10.1103/PhysRev.135.A550>.
- ¹³ A. Larkin and I. Ovchinnikov, *Soviet Physics-JETP* **20**, 762 (1965).
- ¹⁴ D. F. Agterberg, J. S. Davis, S. D. Edkins, E. Fradkin, D. J. Van Harlingen, S. A. Kivelson, P. A. Lee, L. Radzihovsky, J. M. Tranquada, and Y. Wang, *Annual Review of Condensed Matter Physics* **11**, 231–270 (2020), ISSN 1947-5462, URL <http://dx.doi.org/10.1146/annurev-conmatphys-031119-050711>.
- ¹⁵ C. Martin, C. Agosta, S. Tozer, H. Radovan, E. Palm, T. Murphy, and J. Sarrao, *Physical Review B* **71**, 020503 (2005).
- ¹⁶ M. Kenzelmann, T. Strässle, C. Niedermayer, M. Sigrist, B. Padmanabhan, M. Zolliker, A. D. Bianchi, R. Movshovich, E. D. Bauer, J. L. Sarrao, et al., *Science* **321**, 1652 (2008), ISSN 0036-8075, <https://science.sciencemag.org/content/321/5896/1652.full.pdf>, URL <https://science.sciencemag.org/content/321/5896/1652>.
- ¹⁷ V. Kozii, J. W. F. Venderbos, and L. Fu, *Science Advances* **2** (2016), <https://advances.sciencemag.org/content/2/12/e1601835.full.pdf>, URL <https://advances.sciencemag.org/content/2/12/e1601835>.

Appendix A: perfect nesting for spherical Fermi surface

A special example for PDW state is the elliptical Fermi surface with $\varepsilon_{\mathbf{k}} = \sum_i \frac{k_i^2}{2m_i}$. The spin-up and spin-down Fermi surfaces are shifted by $\pm m_x \lambda$, as shown in Fig.A.5. Due to the quadratic dispersion, the final Fermi surfaces are not distorted, which leads to a new Fermi surface perfect nesting. Pairing susceptibility diverges at $q_{x+} = -q_{x-} = 2m_x \lambda$ and $q_{x0} = 0$. In the calculations for surface-bound states, we used a spherical Fermi surface. But we did not focus on Fermi surface perfect nesting, i.e. $\mathbf{q}_{\pm,0}$ are taken to be independent parameters in the model.

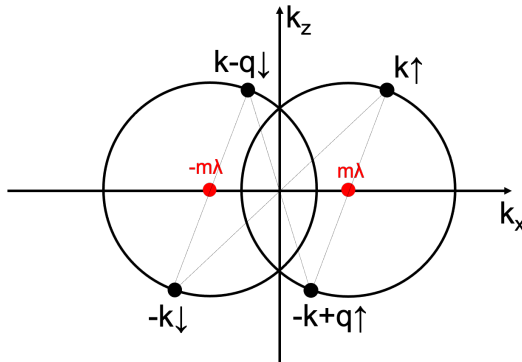


FIG. A.5: Spherical Fermi surface with $\lambda' = 0$, projected to (k_x, k_z) plane. Perfect nesting with $q_{x+} = -q_{x-} = 2m\lambda$ is shown by the dotted line.

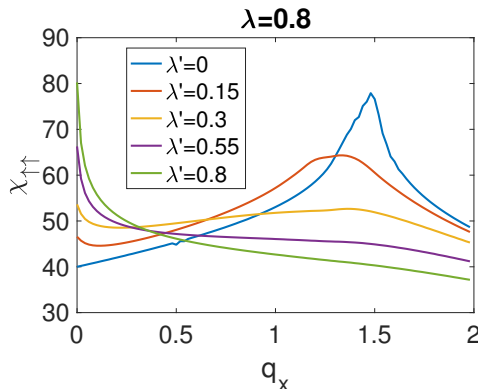


FIG. A.6: Pairing susceptibility for fixed λ with various λ'

Appendix B: pairing susceptibility

For simplicity, we calculated pairing susceptibilities for state $\Delta_{\uparrow\downarrow}^{\mathbf{q}}(\mathbf{k}) = k_z$, with Cooper pair momentum $\mathbf{q} = (q_x, 0, 0)$, while neglecting all other states. The same Hamiltonian and parameters are used as in the caption of Fig.1. The results are shown in Fig.A.6. We found a critical λ' around 0.3. For $\lambda' < 0.3$, pairing susceptibility is maximized at non-zero momentum. For $\lambda' > 0.3$, it is maximized at zero momentum. It is worth noting that, other states certainly play a more important role for larger λ' , and more quantitative analysis including pairing interactions is needed to get a complete phase diagram.

Appendix C: Translational symmetry&coupling to charge-density-wave

Condensate with a single center of mass momentum preserves particle-hole symmetry, as one can always shift the origin of momentum space and let $\mathbf{q} = \mathbf{0}$. To break the translational symmetry and particle-hole symmetry, it is

necessary to have at least two condensate momenta. The difference in these momenta determines the orientation and periodicity of PDW:

$$\Delta(x) \sim \cos\left(\frac{1}{2}\Delta\mathbf{q} \cdot \mathbf{x}\right) \quad (\text{C1})$$

The model generically has more than two condensate momenta. For instance, in the limit of $\lambda' \ll \lambda$, PDW has one Cooper pair momentum in each pairing channel (if ordered). Therefore, we will require at least two pairing channels to be ordered for PH symmetry breaking. An easier possibility is to have ordered $\Delta_{\uparrow\uparrow}$ and $\Delta_{\downarrow\downarrow}$ channels since the competition between them is weak. Other coexisting scenarios will require stronger pairing interactions.

Next, we discuss a consequence of non-uniform superconductivity: the development of charge modulation. The coupling between the charge density wave (CDW) and superconducting order parameters can be deduced from Ginzburg-Landau theory. Gauge invariance constrains the lowest order coupling to be quadratic in Δ :

$$f_{int} = \sum_{ijab} \alpha_{ab}^{ij} \rho_{\mathbf{q}_j - \mathbf{q}_i} \left[\Delta_{\mathbf{q}_i}^{\mathbf{q}_i} (\Delta_{\mathbf{q}_j}^{\mathbf{q}_j})^* + (\Delta_{\mathbf{q}_i}^{-\mathbf{q}_i})^* \Delta_{\mathbf{q}_j}^{-\mathbf{q}_j} \right] \quad (\text{C2})$$

, with proper coefficients α_{ab}^{ij} determined by the normal state dispersion. a, b denotes different pairing channels: $a, b = \uparrow\uparrow, \uparrow\downarrow, \downarrow\downarrow$, while their time-reversal pairs are $a', b' = \downarrow\downarrow, \uparrow\downarrow, \uparrow\uparrow$.

1. special case at $\lambda' = 0$

But right at $\lambda' = 0$, translational symmetry is more subtle. Since the normal state Hamiltonian does not couple spin-up and spin-down states, different channels do not couple in the above equation; i.e. $\alpha_{ab}^{ij} \neq 0$ only for $a = b$. Since there is a unique \mathbf{q} in each pairing channel, the above quadratic terms only couple to uniform charge density, rather than CDW. The actual leading order contribution to CDW is then quartic in Δ :

$$\rho_{\mathbf{q}}^{\uparrow\uparrow}, \rho_{\mathbf{q}}^{\downarrow\downarrow} \propto \left[\Delta_{\mathbf{q}_+}^{\uparrow\uparrow} \Delta_{\mathbf{q}_0}^{\uparrow\downarrow*} \Delta_{\mathbf{q}_-}^{\downarrow\downarrow} \Delta_{\mathbf{q}_0}^{\uparrow\downarrow*} + \Delta_{-\mathbf{q}_+}^{\uparrow\uparrow*} \Delta_{-\mathbf{q}_0}^{\uparrow\downarrow} \Delta_{-\mathbf{q}_-}^{\downarrow\downarrow*} \Delta_{-\mathbf{q}_0}^{\uparrow\downarrow} \right] \quad (\text{C3})$$

$$\mathbf{q} = \mathbf{q}_+ + \mathbf{q}_- - 2\mathbf{q}_0,$$

A non-zero wavevector \mathbf{q} requires $\mathbf{q}_+ + \mathbf{q}_- \neq 2\mathbf{q}_0$, which is the condition of translational symmetry breaking at $\lambda' = 0$. CDW is expected to be weak at $\lambda' = 0$ since it is only contributed by quartic terms in Δ . CDW should be still small in the limit of $\lambda' \ll \lambda$.

Appendix D: $(0, -1, -1)$ and $(0, 1, 1)$ surfaces

In this section, (x, y, z) axes will denote the crystal axes, while (x', y', z') axes are local coordinate set up in Fig.4. The pairing state is taken to be $k_x + ik_y$ state, satisfying the Kerr effect measurement, with the following gap function

$$\vec{d}_0 = (\Delta_3 k_z, i\Delta_4 k_z, \Delta_1 k_x + i\Delta_2 k_y) \quad (\text{D1})$$

As we consider surface bound state on $(0, -1, -1)$ and $(0, 1, 1)$ surfaces, we need to go to the local basis, where y' -axis is normal vector of the top surface, while z' is the normal vector of the side $(0, 1, 1)/(0, -1, -1)$ surface. x' -axis is the same as crystal x -axis. Basis transformation leads to a vector rotation on both \mathbf{k} and a vector rotation of the d -vector:

$$\vec{d}(\mathbf{k}') = M\vec{d}_0(M\mathbf{k}) \quad (\text{D2})$$

, where matrix M is the standard rotation matrix in 3D.

Now we can calculate surface-bound states on the two side surfaces, and the results is shown below:

We observed that the peak in LDOS on the two surfaces should be located at different energies. But LDOS profile is not the same.

